sufficient numbers of particles to slip into acceleration phase and this terminates the growth of the electromagnetic wave. In the varying ripple case the pondermotive force becomes so strong that more than half of the particles are pushed into the bottom of the deep potential well. At this instant the beam kinetic energy is a minimum which, from conservation of energy, gives rise to maximum radiation. However, the average beam particles are in the accelerating phase relative to the EM wave and they gain energy from the wave. This results in oscillation in the bulk particle distribution and eventually the distribution becomes thermalized. In the end, the beam gives up a lot more kinetic energy in comparison with the constant ripple case. However, the device length should be terminated at the first peak of the radiation to obtain the maximum efficiency at the desired frequency.

In conclusion, we proposed that by properly varying the ripple strength of a free-electron laser, the efficiency can be substantially increased along with some other benefits such as narrow bandwidth and shortening of the length of the device. The performance might be improved further by optimizing the form of the varying ripple strength.

It is a great pleasure to acknowledge the extensive numerical work performed by Mrs. Chih-Chien Lin. This work was supported by the National Science Foundation Contract No. PHY 76-83686 and U. S. Department of Energy Contract No. EY-76-C-03-0010.

[1]H. Motz, in *Proceedings of the Symposium on Millimeter Waves, Microwave Research Institute Symposia Series*, edited by J. Fox (Interscience, New York, 1960), Vol. IX, p. 155.

[2]R. H. Pantell, G. Soncini, and H. E. Puthoff, IEEE J. Quantum Electron. 6, 905 (1968).

[3]D. A. G. Deacon, L. R. Elias, J. M. J. Madey, G. J. Ramain, H. A. Schwettman, and T. I. Smith, Phys. Rev. Lett. 38, 892 (1977).

[4]D. B. McDermott, T. C. Marshall, S. P. Schlesinger, R. K. Parker, and V. L. Granatstein, Phys. Rev. Lett. 41, 1368 (1978).

[5]P. Sprangle, V. L. Granatstein and L. Baker, Phys. Rev. A 12, 1697 (1975).

[6]V. L. Granatstein and P. Sprangle, IEEE Trans. Microwave Theory Tech. 25, 545 (1977).

[7]I. B. Bernstein and J. L. Hirshfield, Phys. Rev. Lett. 40, 761 (1978).

[8]D. Forslund, J. Kindel, and E. Lindman, Phys. Rev. Lett. 30, 739 (1973).

[9]F. A. Hopf, P. Meystre, M. O. Scully, and W. H. Louisell, Phys. Rev. Lett. 37, 1342 (1976), and 39, 1496(E) (1977).

[10]T. Kwan, J. M. Dawson, and A. T. Lin, Phys. Fluids 20, 581 (1977).

[11]P. Sprangle, R. Smith, and V. L. Granatstein, Bull. Am. Phys. Soc. 23, 749 (1978).

[12]J. E. Rowe, *Nonlinear Electron-Wave Interaction Phenomena* (Academic, New York, 1965).

[13]T. Kwan and J. M. Dawson, to be published.

[14]In our previous publication (Ref. 10), the reported efficiency of 28.9% for the case using the same parameters as here the total electromagnetic radiation was included; both high- and low-frequency components were included. The present results of 24% contain only the high-frequency radiation.

Ablative Acceleration of Laser-Irradiated Thin-Foil Targets

R. Decoste,[a] S. E. Bodner, B. H. Ripin, E. A. McLean, S. P. Obenschain,[a] and C. M. Armstrong[b]
Naval Research Laboratory, Washington, D. C. 20375
(Received 20 December 1978)

Ablative acceleration of thin-foil targets at low laser irradiance (10^{12}–10^{13} W/cm^2) is studied experimentally and theoretically. Ablative acceleration of foils up to $\sim 10^7$ cm/sec with good hydrodynamic efficiency (20%) has been achieved. These and other results are in good agreement with a simple rocket model.

In the laser-fusion concept, the near-isentropic implosion of the pellet fuel is driven by the rocketlike ablation of the pellet shell. Pellet-design considerations suggest that acceleration of the shell to a velocity of $\sim 2\times10^7$ cm/sec is sufficient to achieve thermonuclear ignition.[1] We demonstrate, here, *ablative* acceleration (10^{15} cm/sec^2) of thin-foil targets to velocities comparable to those required ($\sim 1\times10^7$ cm/sec) with good hydrodynamic efficiency ($\sim 20\%$).

Thin planar foils, rather than spherical pellets, are used in our experiments in order to have good

access to the rear as well as the laser side of accelerated foils.[2] The laser intensity at 1.06 μm is chosen below 10^{14} W/cm^2 to maximize the ablation efficiency and laser-light absorption. An array of small calorimeters and time-of-flight particle detectors surround the target to measure ablation variables. Also, the structure and behavior of the rear target surface is studied with several optical diagnostics to confirm the acceleration and to provide information about spatial and velocity distributions across the accelerating target. The hydrodynamic behavior is found to be consistent with a simple analytical model.

In this paper, we compare our results to a simple model which treats the one-dimensional ablative acceleration of the target analogously to that of a rocket. During the acceleration phase, the target (rocket) with mass M and velocity v is accelerated by the steady-state blowoff (exhaust) of the ablated plasma (propellant) at a constant velocity u in the target reference frame [Fig. 1(a)], i.e., $Mdv/dt = -udM/dt$. This relation is integrated to yield the well-known rocket equation,[3]

$$v/u = \ln(M_0/M), \tag{1}$$

where M_0 is the initial target mass. The hydrodynamic efficiency η_h is defined as the directed energy of the accelerated foil divided by the absorbed laser energy, i.e., $\eta_h = \frac{1}{2}Mv^2/E_a$. Using Eq. (1) and the fact that the rate of absorbed laser energy must be balanced by the energy dissipated in the ablation and acceleration of the target (neglecting radiative losses, as justified experimentally[2]), we obtain the hydrodynamic efficiency

$$\eta_h = (v/u)^2[\exp(v/u) - 1]^{-1}. \tag{2}$$

For small fractional mass loss, these equations reduce to

$$\eta_h \cong v/u \cong \Delta M/M_0, \tag{3}$$

where $\Delta M = M_0 - M$. Note that the continuity equation allows us to use the asymptotic velocity u for the ablation velocity in Eq. (2). In the asymptotic velocity region, the thermal-energy density (and pressure) is negligible with respect to the directed kinetic energy of expansion. Thermal-energy–transport assumptions[4,5] can therefore be avoided in this model and only a knowledge of the asymptotic ablation velocity (experimentally determined) is required. This approach is possible only in a situation that approximates steady state, which is experimentally observed as a single well-defined asymptotic ablation velocity for Nd-laser pulses over 1-nsec duration.[6]

Equations (1) and (2), which relate the ablation variables, are plotted in Fig. 2(b) (solid lines). When the target velocity becomes comparable to the ablation velocity, the hydrodynamic efficiency increases to a maximum of 65%, and 80% of the initial mass is ablated.[7] However, the data presented below are obtained for cases where Eq. (3) applies, i.e., for $v/u < 1$.

The ablation pressure (thrust) P_a exerted on the target (rocket) by ablation, for one-dimensional ablation, is given by mdv/dt, where m is mass per unit area. Combining this with the energy equation, $I_a = -\frac{1}{2}u^2 dM/dt$, where I_a is the absorbed laser flux, yields the relation

$$P_a = 2I_a/u. \tag{4}$$

For the laser-fusion application, an important consideration is to optimize the hydrodynamic efficiency by varying the pressure or irradiance. Since the function $u(I_a)$ can be determined experimentally, then both P_a and η_h are functions of the laser intensity. Pellet-design considerations fix the final pellet-implosion velocity v, and therefore define the relationship between η_h and P_a for a given laser wavelength. Figure 1(b) shows a hypothetical example. As the laser flux decreases, the ablation pressure decreases and the efficiency (and thus pellet gain) increases. However, since the hydrodynamic stability of an imploding pellet shell decreases with larger shell aspect ratio $R/\Delta R$, and the required P_a is in-

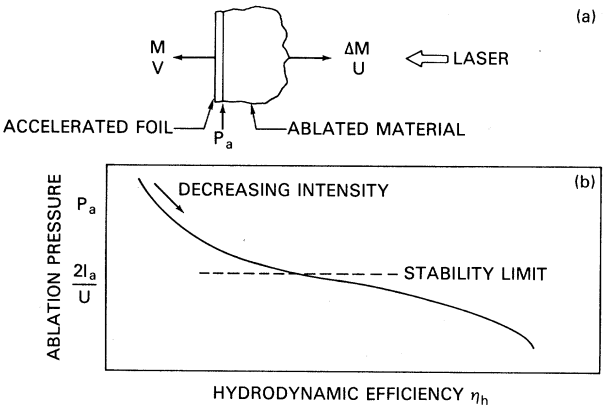

FIG. 1. (a) Ablative acceleration of thin foils. The ion ablation velocity u is defined in the accelerated foil frame. (b) Schematic relationship between ablation pressure and hydrodynamic efficiency. Targets can be stably accelerated above the dashed line.

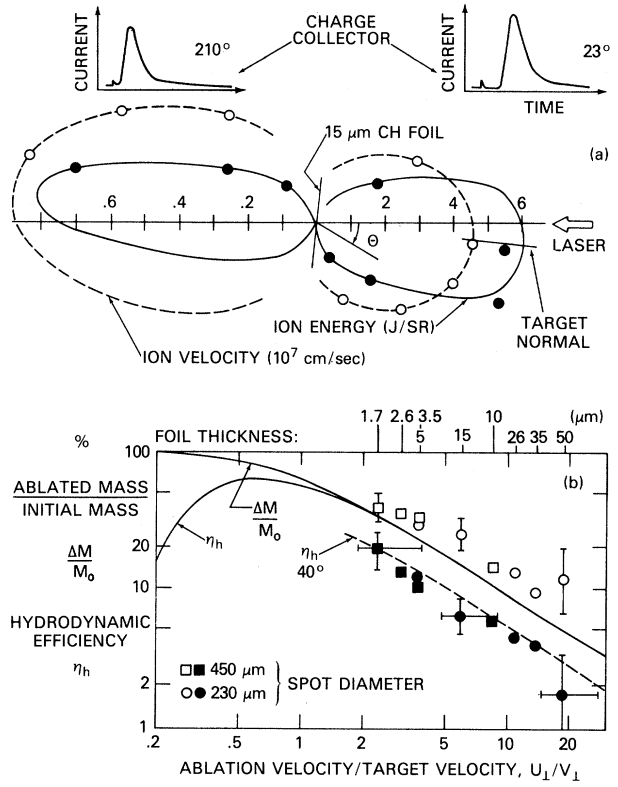

FIG. 2. (a) Typical ablative acceleration data. The average ion ablation velocity u, the final target velocity v, the hydrodynamic efficiency η_h, and the mass fraction ablated $\Delta M/M_0$ are inferred from the angular distributions of energy and velocity. Note the change of scales on the rear versus the front. For this example the Nd-laser parameters were 1×10^{13} W/cm^2 over a 230-μm spot diameter for 3 nsec (full width at half maximum). (b) Ablative acceleration: comparison of experiment and model. Filled and open data points correspond, respectively, to η_h and $\Delta M/M_0$. Experiments were done with varying foil thickness and spot diameters. The error bars are the larger of either a standard deviation or estimated measurement uncertainties.

versely proportional to $R/\Delta R$, there is a lower limit to the pressure that can be applied to the shell, given by the Rayleigh-Taylor instability (dashed line). Our experiments are a first attempt to find that optimal irradiance for 1.06-μm radiation which maximizes efficiency with acceptable stability.

Several diagnostics are used in these studies to measure the ablation and acceleration properties required for a comparison with the model. Thin-foil targets are irradiated at $(0.3-1)\times10^{13}$ W/cm^2 through an aspheric $f/10$, 1-m lens by locating the target several millimeters out of best focus towards the lens, thereby increasing the area and uniformity of illumination. Both the spatial and temporal focal distributions are known over four decades in intensity.[2] Laser-light absorption exceeds 80% as measured with a box calorimeter and discrete minicalorimeters.[2] Figure 2(a) is a typical example of ablative acceleration data for a 15-μm-thick CH foil at 10^{13} W/cm^2. The angular distributions of the ion energy and velocity for the ablation on the laser side, and for the accelerated target material, are measured with the minicalorimeters and time-of-flight detectors. The time-of-flight detectors exhibit single narrow velocity distributions characteristic of ablation[4] (on the laser side) and of the accelerated target debris (on the rear side). The observed average ion ablation velocity u (3.3×10^7 cm/sec, averaged over all angles on the laser side), and the final average target velocity (5.1×10^6 cm/sec) are consistent with results obtained using the optical diagnostics discussed below. The hydrodynamic efficiency η_h (6.6%) is obtained directly from the integration of the angular energy distributions. Finally, the fraction of the mass ablated (0.25) is inferred from the angular integration of the energy divided by the square of the velocity.

Other experimental results for different target thicknesses and irradiances are shown in Fig. 2(b), together with a comparison with the rocket model. For a given irradiance, different values for the final target velocities, the mass fractions ablated, and hydrodynamic efficiencies are obtained by varying only the initial foil thickness. The ablated mass and ablation velocities are functions only of irradiance and pulse duration since, here, $u/v>1$. Experiments are done at 1×10^{13} W/cm^2 and 3×10^{12} W/cm^2 with respective laser-spot diameters of 230 and 450 μm. The corresponding average ablation velocities are 3.3×10^7 cm/sec and 2.5×10^7 cm/sec. The dashed line in Fig. 2(b) is a correction introduced in the one-dimensional model to account for the experimentally observed effective ion blowoff angle of 40° to the target normal. Accordingly, only the ablation and target velocities normal to the target surface are compared in Fig. 2(b). The high absorption fraction of the incident laser light (80%) combined with the efficient (~20%) ablative acceleration to high velocity (~1×10^7 cm/sec) observed is encouraging for the ablative acceleration of a pellet shell to fusion velocities. Moreover, the target velocities achieved here already exceed the velocities required for injection of pellet fuels into a magnetic fusion power reactor.[7]

Edge effects become important when thin targets are accelerated a distance comparable to the laser-spot diameter. In this case, a significant fraction of the laser energy flows toward the side as well as towards the accelerated target. Edge effects are experimentally observed as an increase in the effective diameter of ablated material exceeding the laser-spot size with a corresponding decrease in the thickness of ablated material. In Fig. 2(b), edge effects become important when the target thickness is less than 15 and 3.5 μm for laser-spot diameters of 230 and 450 μm, respectively. It should be emphasized, however, that the scaling between the ablation variables [Eqs. (1) and (2)] is still valid even when the thickness of ablated material becomes dependent on target thickness. Measurements of edge effects, and lateral and axial heat transport are described in Ref. 2.

The ablation pressures inferred from Eq. (4) are, respectively, 1 and 3 Mbar, for the 450- and 230-μm laser-spot-size cases (irradiances of 3×10^{12} and 1×10^{13} W/cm^2) where edge effects are negligible.

The structure and behavior of the rear surface of the foil were observed during the acceleration phase with optical diagnostics. Figure 3(a) shows three edge-view shadowgram frames, taken with a short-duration probe beam (~ 400 psec, 5320 Å) at different times with respect to the peak of the main laser pulse. From a series of such shadowgrams, the displacement and, consequently, the velocity of the rear surface are obtained as a function of time. Velocity measurements from frame and streak shadowgraphy, as well as an asymptotic velocity obtained from Fig. 2(a) are compared in Fig. 3(b). The streak shadowgraphy data are obtained using the nonshortened 5320-Å probing beam as a backlighting source. The smooth and continuous acceleration of the rear surface seen in Fig. 3(b) (~ 10^{15} cm/sec^2) is consistent with the applied pressure inferred from Eq. (4), and cannot be easily explained by other phenomena such as shock wave or spallation. The Doppler shift, and thus velocity of the cold rear surface of the target are measured by imaging the short-duration probe light reflected from the rear target surface onto the entrance slit of a stigmatic spectrograph. Figure 3(c) shows the Doppler inferred velocity profiles 0.8 nsec before and 0.2 nsec after the peak of the main laser pulse for a 7-μm-thick Al target. At the later time, a slug of material comparable to the laser-spot size has apparently broken away from the rest of the target and is accelerated to a nearly spatially uniform velocity of ~ 10^6 cm/sec, consistent with the model and the other determinations.

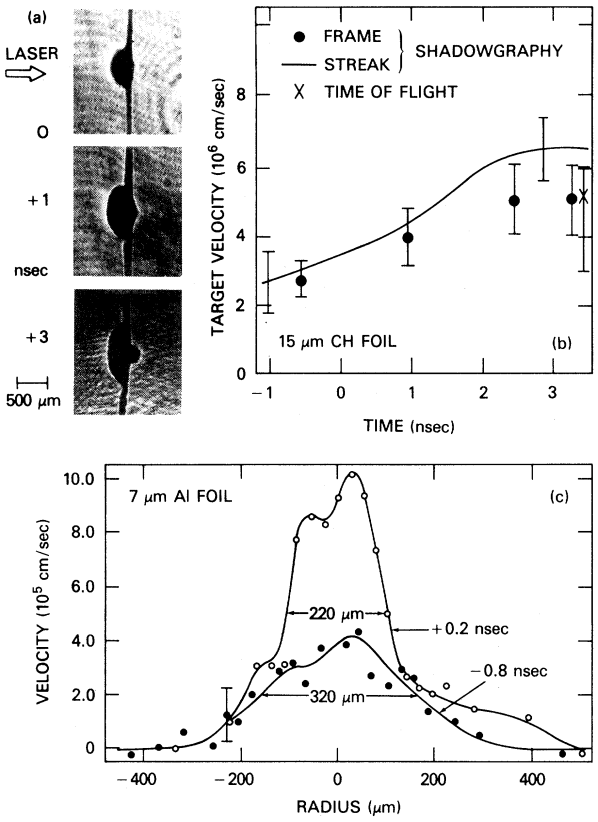

FIG. 3. Dynamics of ablatively accelerated targets. (a) Frame shadowgrams of irradiated CH foils at selected times with respect to the peak of the laser pulse. (b) Rear surface velocity vs time obtained with streak (solid line) and frame (filled circles) shadowgraphy, and an asymptotic time-of-flight velocity determination. (c) Doppler-shift velocity profiles across the rear surface of a 7-μm Al target for the same laser parameters as in (b) above and Fig. 2(a). Note that the full width at half maximum of the velocity profile at +0.2 nsec is equal to the laser-spot size within experimental accuracy.

To conclude, it has been shown that in the long-pulse, low-irradiance regime considered here, thin-foil targets have been *ablatively* accelerated up to ~ 10^7 cm/sec, within a factor of 2 of what is required for pellet ignition, with a good hydrodynamic efficiency (~20%). These results are in reasonable agreement with the simple analogy to a rocket and are encouraging for the laser-fusion application. Future experiments will deal more fully with laser-beam uniformity requirements and the stability of the accelerated foils.

The authors gratefully acknowledge the contributions of J. Boris, P. Moffa, S. H. Gold, J. Grun, J. A. Stamper, R. R. Whitlock, and F. C. Young. This work is sponsored by the U. S. Department of Energy.

---

[a] Present association: Sachs/Freeman Associates, Bladensburg, Md.

[b] Present address: North Carolina State University, Raleigh, N. C. 27650.

[1] D. Henderson, private communication; J. H. Nuckolls *et al.*, in European Conference on Laser Interaction with Matter, Oxford, England, 1977 (unpublished).

[2] For a detailed discussion, see Naval Research Laboratories Laser-Plasma Interaction Group, NRL Memo Report No. 3890, December 1978, edited by B. H. Ripin (unpublished); also, B. H. Ripin, R. R. Whitlock, F. C. Young, S. P. Obenschain, E. A. McLean, and R. Decoste, NRL Memo Report No. 3965, February 1979 (to be published).

[3] R. Resnick and D. Halliday, *Physics* (Wiley, New York, 1978), Vol. I, p. 178.

[4] K. A. Brueckner and A. Jorna, Rev. Mod. Phys. 46, 325 (1974); T. R. Jorboe, W. B. Kundeband, and A. F. Lietzke, Phys. Fluids 19, 1501 (1976); F. S. Felber, Phys. Rev. Lett. 29, 84 (1977); S. J. Gitomer, R. L. Morse, and B. S. Newberger, Phys. Fluids 20, 234 (1977).

[5] J. P. Anthes, M. A. Gusinow, and M. K. Matzen, Phys. Rev. Lett. 41, 1300 (1978); M. A. Gusinow, J. P. Anthes, M. K. Matzen, and D. Woodall, Appl. Phys. Lett. 33, 800 (1978).

[6] M. K. Matzen and R. K. Morse, Phys. Fluids 22, 654 (1979); P. J. Moffa, J. H. Orens, and J. P. Boris (to be published).

[7] F. S. Felber, Nucl. Fusion 18, 1469 (1978); T. E. McCann and J. S. DeGroot, Bull. Am. Phys. Soc. 22, 1205 (1977).

Consistency of the α-Effect Turbulent Dynamo

Robert H. Kraichnan
Dublin, New Hampshire 03444
(Received 5 March 1979)

The paradox of the infinite-conductivity α-effect dynamo is resolved by properly treating the boundary layer. If the turbulence is not too intermittent the expansion of the mean electromotive force in powers of the wave number of the mean magnetic field $\vec{B}$ is found to converge, and the usual truncation gives little error. The α effect is demonstrated in the strong-field limit where the turbulence consists of Alfvén waves propagating along $\vec{B}$.

The amplification of large-scale magnetic fields by helical turbulence in a conducting fluid (α effect) has been extensively investigated since the physical mechanism was proposed by Parker.[1-3] If Lorentz forces are neglected, the quasilinear or first-order smoothing approximation (QLA) yields the α-effect equation[1-5]

$$\partial\vec{B}/\partial t = \eta\nabla^2\vec{B} - \alpha\nabla\times\vec{B}, \tag{1}$$

where $\vec{B}$ is the ensemble-average (mean) induction field and, if conductivity σ is sufficiently large, α and η are related to the rms turbulent velocity v_0, correlation length k_0^{-1}, and correlation time $t_* \lesssim 1/v_0k_0$ of a prescribed statistically isotropic and homogeneous turbulence field by

$$|\alpha| \lesssim v_0^2k_0t_*, \quad \eta \sim v_0^2t_*. \tag{2}$$

In mirror-symmetric turbulence, α vanishes. A more elaborate approximation[5] predicts that η can be negative, its magnitude given by (2), in mirror-symmetric turbulence with strong helicity fluctuations that persist over domains several correlation lengths and times in extent.

In this note I discuss the following questions: (i) Do (1) and (2) imply violation of flux conservation through a circuit moving with the fluid if $\sigma = \infty$? (ii) Can higher spatial derivatives of $\vec{B}$, omitted in (1), really be neglected? (iii) Does the α effect survive when Lorentz forces are strong?

Krause and Steenbeck[2] have described axially symmetric solutions of (1) in which the total magnetic flux through a conducting fluid sphere in vacuum increases exponentially with time under the boundary condition of continuous $\vec{B}$ at the surface of the sphere. Moffatt[6] points out that this is paradoxical in the limit $\sigma = \infty$ since the flux enclosed by the equator of the sphere cannot then change with time so that, according to Bondi and Gold,[7] the dipole moment is bounded. The paradox is already present if $\alpha = 0$ because in this case also (1) gives a change of total flux even if

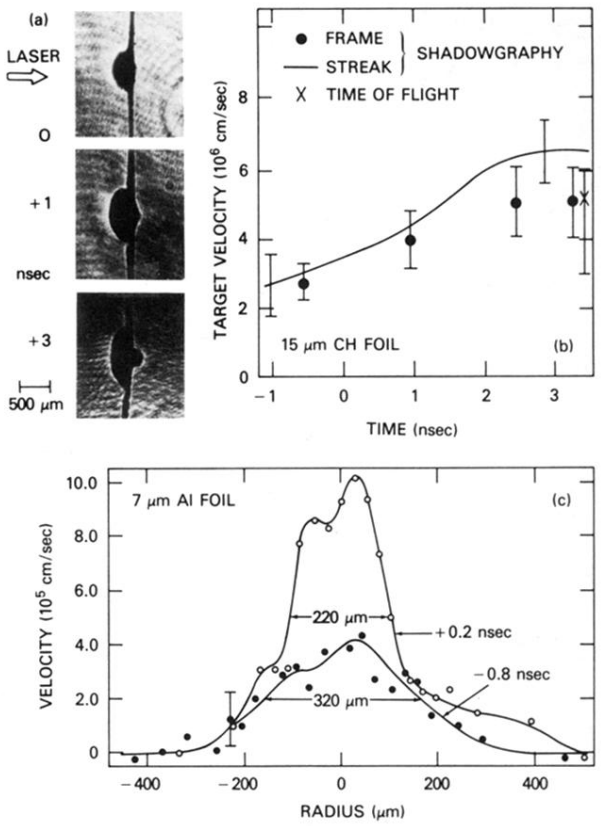

FIG. 3. Dynamics of ablatively accelerated targets. (a) Frame shadowgrams of irradiated CH foils at selected times with respect to the peak of the laser pulse. (b) Rear surface velocity vs time obtained with streak (solid line) and frame (filled circles) shadowgraphy, and an asymptotic time-of-flight velocity determination. (c) Doppler-shift velocity profiles across the rear surface of a 7-μm Al target for the same laser parameters as in (b) above and Fig. 2(a). Note that the full width at half maximum of the velocity profile at +0.2 nsec is equal to the laser-spot size within experimental accuracy.